Supporting Information

Molecular recognition of a host protein by NS1 of pandemic and seasonal influenza A viruses

Jae-Hyun Cho[1,*], Baoyu Zhao[1], Jie Shi[2], Nowlan Savage[1], Qingliang Shen[1], James Byrnes[3], Lin Yang[3], Wonmuk Hwang[2,4,5,6], Pingwei Li[1]

[1]Department of Biochemistry and Biophysics, Texas A&M University, College Station, TX 77843, USA

[2]Department of Biomedical Engineering, Texas A&M University, College Station, TX 77843, USA

[3]National Synchrotron Light Source II, Brookhaven National Laboratory, Upton, NY 11973, USA

[4]Department of Materials Science and Engineering, Texas A&M University, College Station, TX 77843, USA

[5]Department of Physics and Astronomy, Texas A&M University, College Station, TX 77843, USA

[6]School of Computational Sciences, Korea Institute for Advanced Study, Seoul 02455, Korea

*Correspondence and requests for materials should be addressed to J.H.C. (email: jaehyuncho@tamu.edu)

www.pnas.org/cgi/doi/10.1073/pnas.1920582117

Supporting Table 1

Table S1. X-ray diffraction and refinement statistics of the complexes of 1918 NS^{ED} and $p85\beta^{iSH2}$.

	1918 NS1-ED W187A PDB ID: 6U28	**1918 NS1-ED W187R** PDB ID: 6OX7
Data collection*		
Space group	$P2_1$	$P2_1$
Cell dimensions		
a, *b*, *c* (Å)	61.19, 92.39, 66.94	60.98, 94.03, 67.22
α, β, γ (°)	90.00, 105.17, 90.00	90.00, 105.31, 90.00
Resolution (Å)	2.95 (3.13 to 2.95)**	2.75 (2.90 to 2.75)**
R_{merge}	0.179 (0.938)	0.163 (0.623)
R_{pim}	0.111 (0.587)	0.099 (0.379)
$I / \sigma I$	6.1 (1.3)	6.7 (2.1)
Completeness (%)	100 (100)	100 (100)
Redundancy	3.5 (3.5)	3.7 (3.7)
Refinement		
Resolution (Å)	2.95	2.75
No. Reflections	15214	19103
R_{work}/R_{free}	0.223/0.240	0.228/0.263
No. atoms		
Protein	4219	4231
Water	0	34
B-factors (Å^2)		
Overall	74.0	60.8
R.m.s. deviations		
Bond lengths (Å)	0.002	0.002
Bond angles (°)	0.489	0.449

* The numbers in parentheses refer to the highest resolution shell.
** A single crystal was sued to collect each of the dataset.

Supporting Figure 1

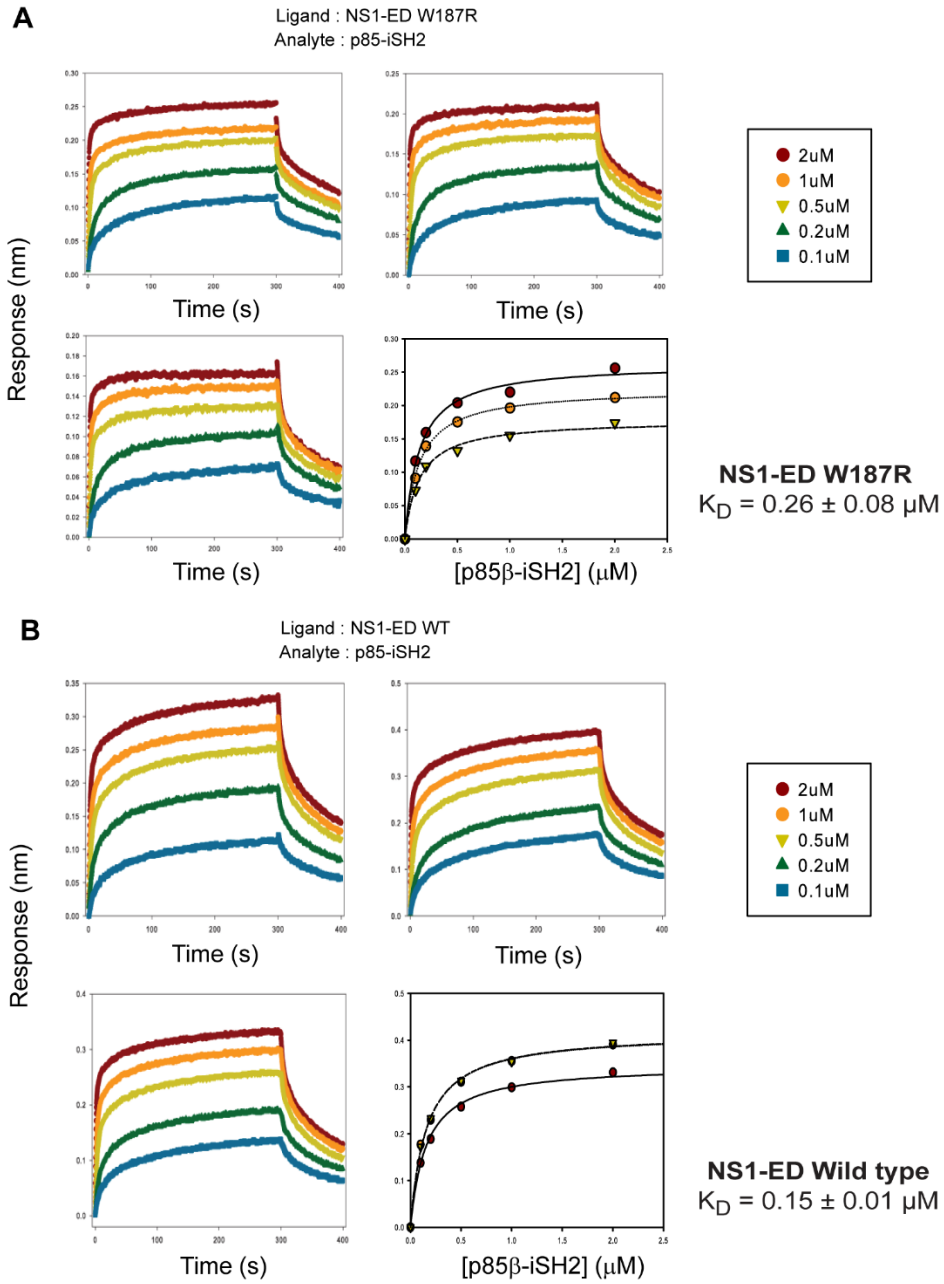

Figure S1. BLI sensorgrams and binding isotherms (**A**) between surface-immobilized 1918 $NS1^{ED}$ W187R and free $p85\beta^{iSH2}$ in wells and (**B**) between surface-immobilized 1918 $NS1^{ED}$ wild type and free $p85\beta^{iSH2}$ in wells. The binding isotherms were globally fit to obtain binding affinities (K_D).

Supporting Figure 2.

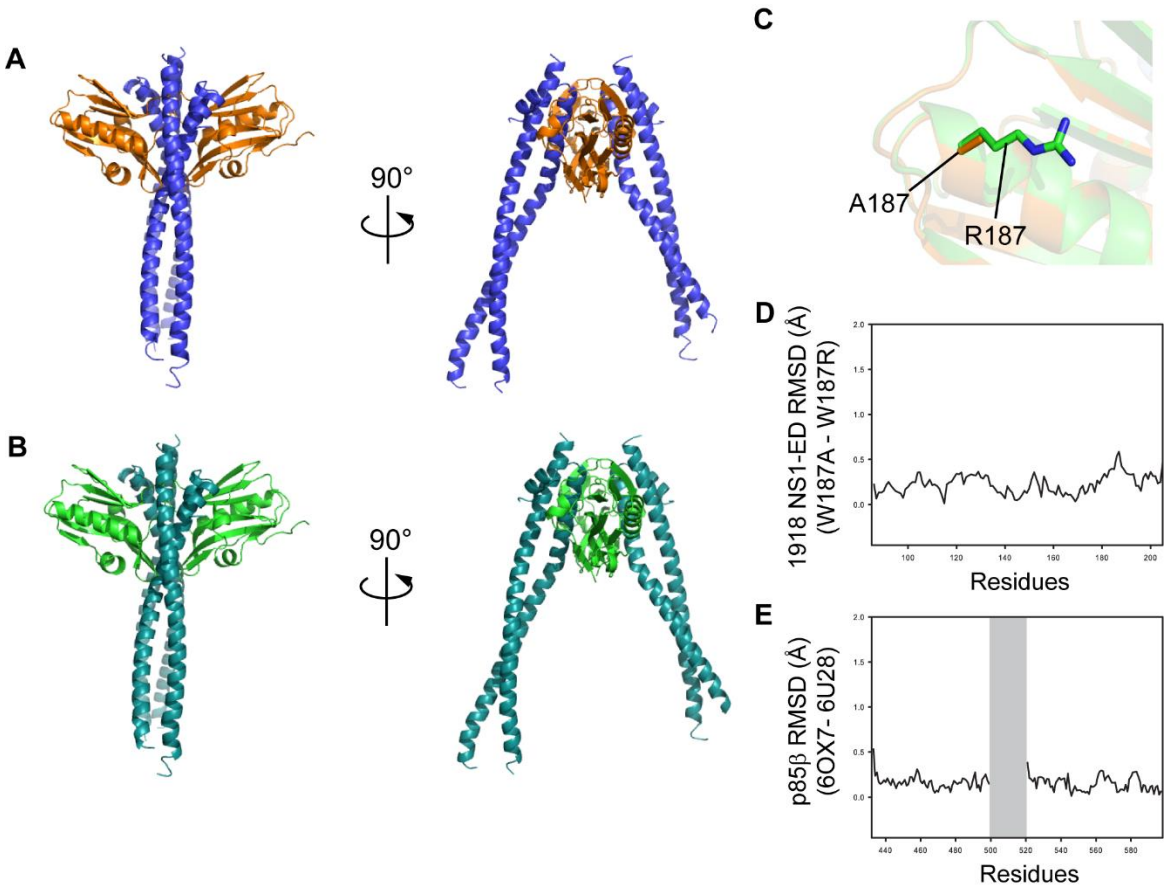

F

	Interface Residues
1918 NS1 ED	S87, R88, Y89, T91, M93, L95, E96, E97, M98, S99, R100, D101, C116, F134, S135, T143, L144, I145, L146, R148, E159 S161, P162, P164, S165
p85β-iSH2	M568, R571, K572, R574, D575, Q576, L578, V579, W580, T582, Q583 K584, R587, Q588, L595

Figure S2. Crystal structures of the complexes between (**A**) 1918 NS1^{ED} W187A (orange) and p85β^{iSH2} (blue) (PDB ID: 6U28) and (**B**) 1918 NS1^{ED} W187R (green) and p85β^{iSH2} (deep teal) (PDB ID: 6OX7). (**C**) Superimposed structures of NS1-ED in the two complexes. Side chains of A187 and R187 are shown in orange and green stick models, respectively. RMSD plots of (**D**) 1918 NS1^{ED} and (**E**) p85β between the two complex structures. Electron densities corresponding to residues 500 – 520 are missing (gray) in both crystal structures. (**F**) Residues in the complex interface between 1918 NS1^{ED} and p85β^{iSH2}.

Supporting Figure 3

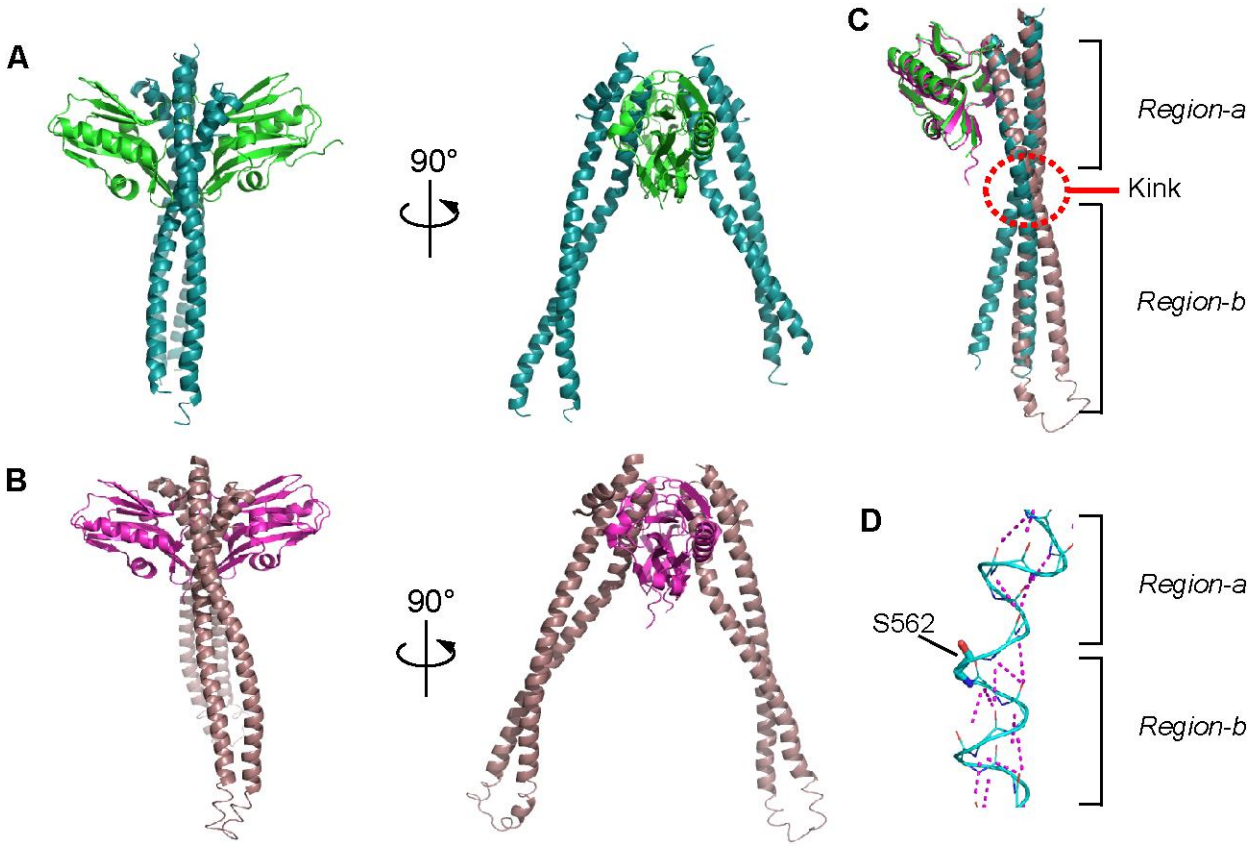

Figure S3. Structure comparison between 1918 $NS1^{ED}$ and PR8 $NS1^{ED}$ in complex with p85β. Crystal structure of the complex between (**A**) 1918 $NS1^{ED}$ and human $p85\beta^{iSH2}$ (PDB ID: 6U28) and (**B**) PR8 $NS1^{ED}$ and bovine $p85\beta^{iSH2}$ (PDB ID: 3L4Q). (**C**) Superposed structures of the two complexes. For clarity, only one complex molecule from each complex is superimposed. The color schemes are same as in (A) and (B). Both $p85\beta^{iSH2}$ proteins form a kinked coiled-coil conformation. Therefore, $p85\beta^{iSH2}$ can be distinguished by two regions: region-a (residues 433 – 453 and 563 – 597), which includes the NS1-binding region (residues 565 – 597) and region-b which includes the rest of the domains (residues 454 – 562). (**D**) The kinked conformation is due to that an intramolecular backbone hydrogen bond is missing at S562 in human protein (S556 in bovine protein sequence). Dotted lines (magenta) correspond to backbone hydrogen bonds. Due the missing hydrogen bond, the region-b has high conformational mobility, resulting in large RMSD between the two complexes.

Supplementary Figure 4

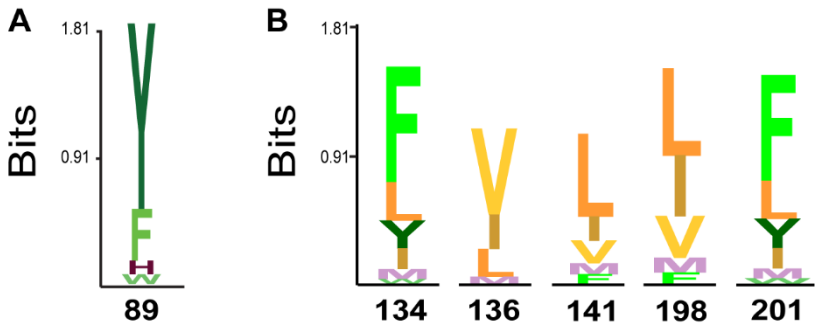

Figure S4. Sequence logo illustrating the conservation of (**A**) Y89 and (**B**) hydrophobic residues in all known human IAVs (see Materials and Methods).

Supporting Figure 5.

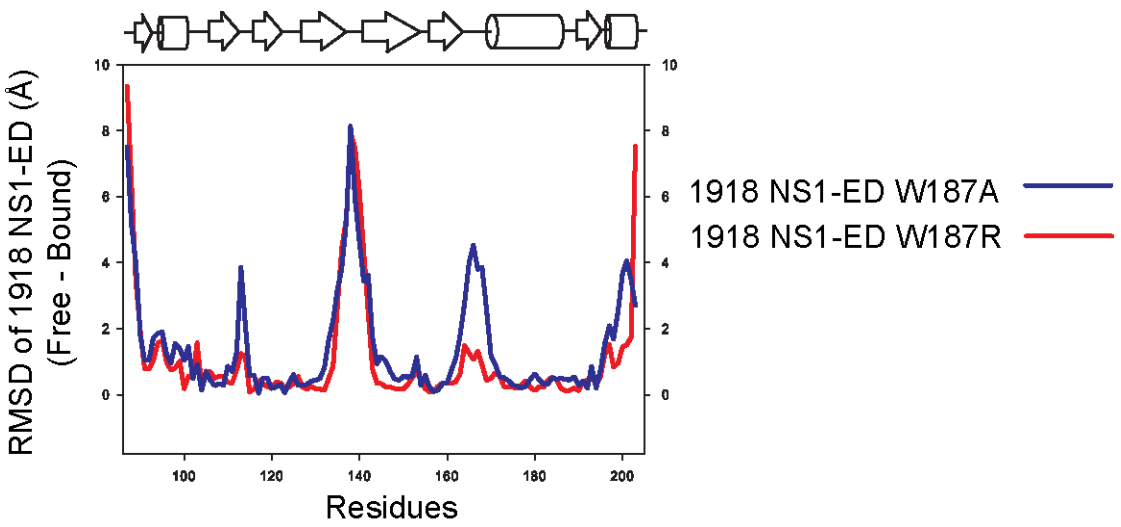

Figure S5. RMSD plots of 1918 NS1^{ED} W187A (blue line) and W187R (red line) between the free and p85β-bound forms. Following structures were used to calculate RMSD values; free 1918 NS1^{ED} W187A (PDB ID: 6DGK), free 1918 NS1^{ED} W187R (PDB ID: 6NU0), p85β-bound W187A (PDB ID: 6U28), and p85β-bound W187R (PDB ID: 6OX7).

Supporting Figure 6.

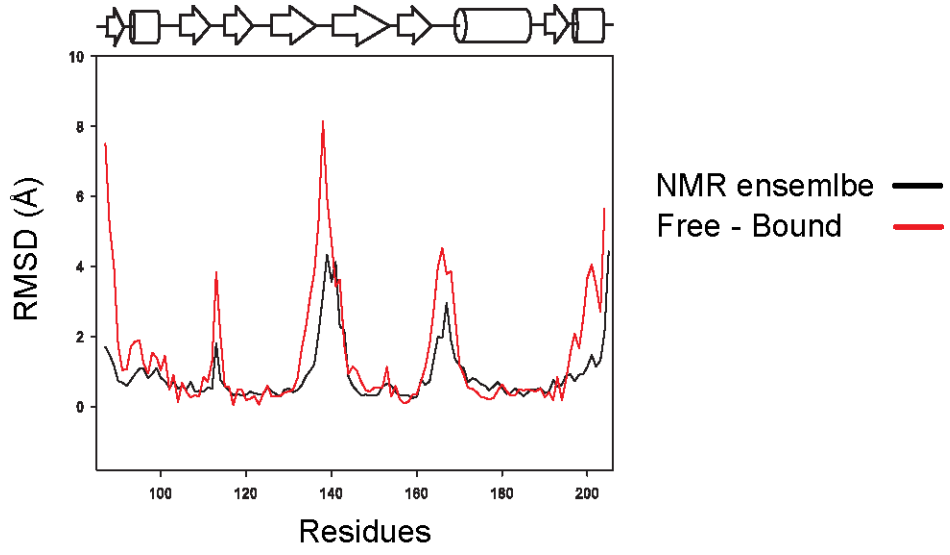

Figure S6. Structurally plastic regions in free 1918 NS1^{ED} overlap with the regions undergoing conformational change upon binding p85β. RMSD plot of 1918 NS1^{ED} between the free and p85β-bound forms and average RMSD of the 20 lowest energy structures in the NMR ensemble are shown in red and black lines, respectively.

Supporting Figure 7A

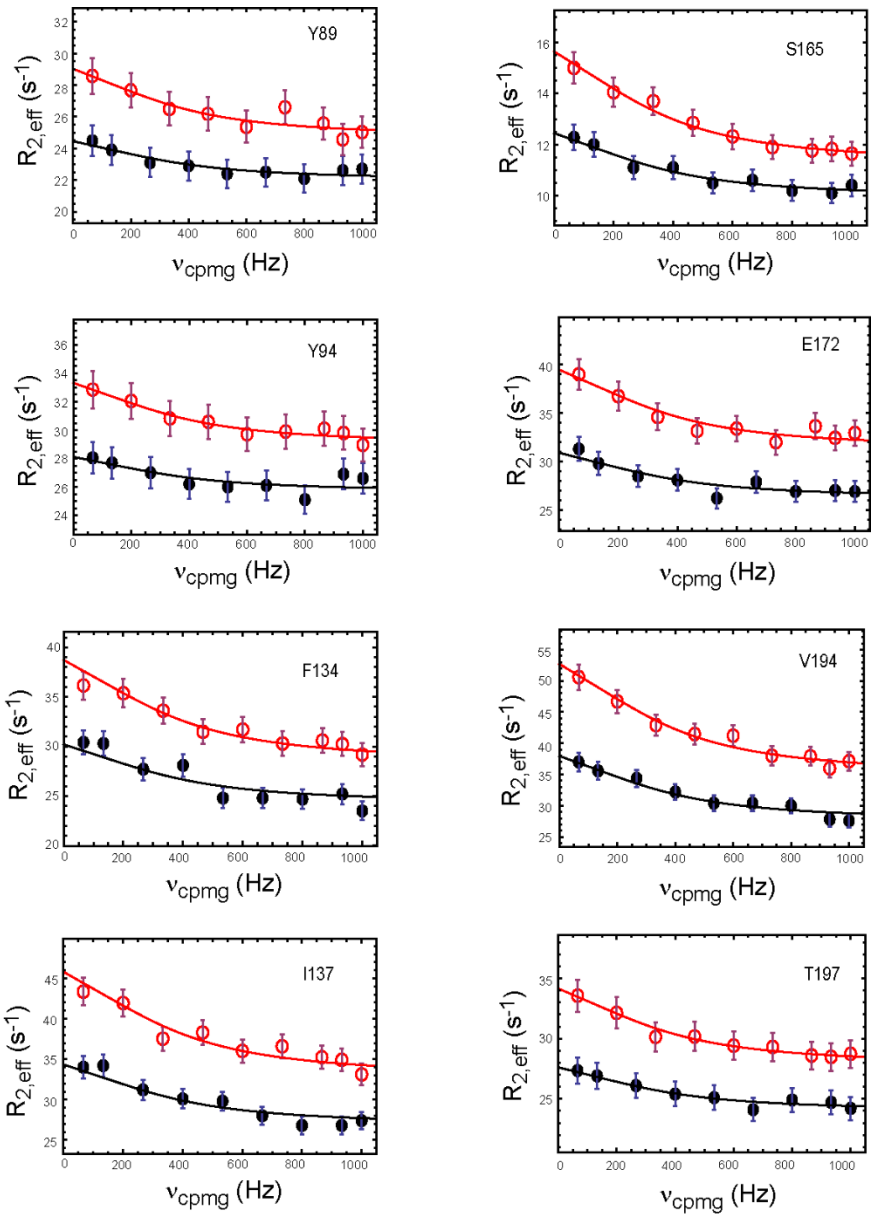

Figure S7A. NMR CPMG-RD data of residues in group-A. Data at both field strengths were globally fit (solid lines) using the Carver-Richards equation with an assumption of a simple two-state exchange model. The global fitting yielded k_{ex} = 2459 ± 205 s^{-1}.

Supporting Figure 7B

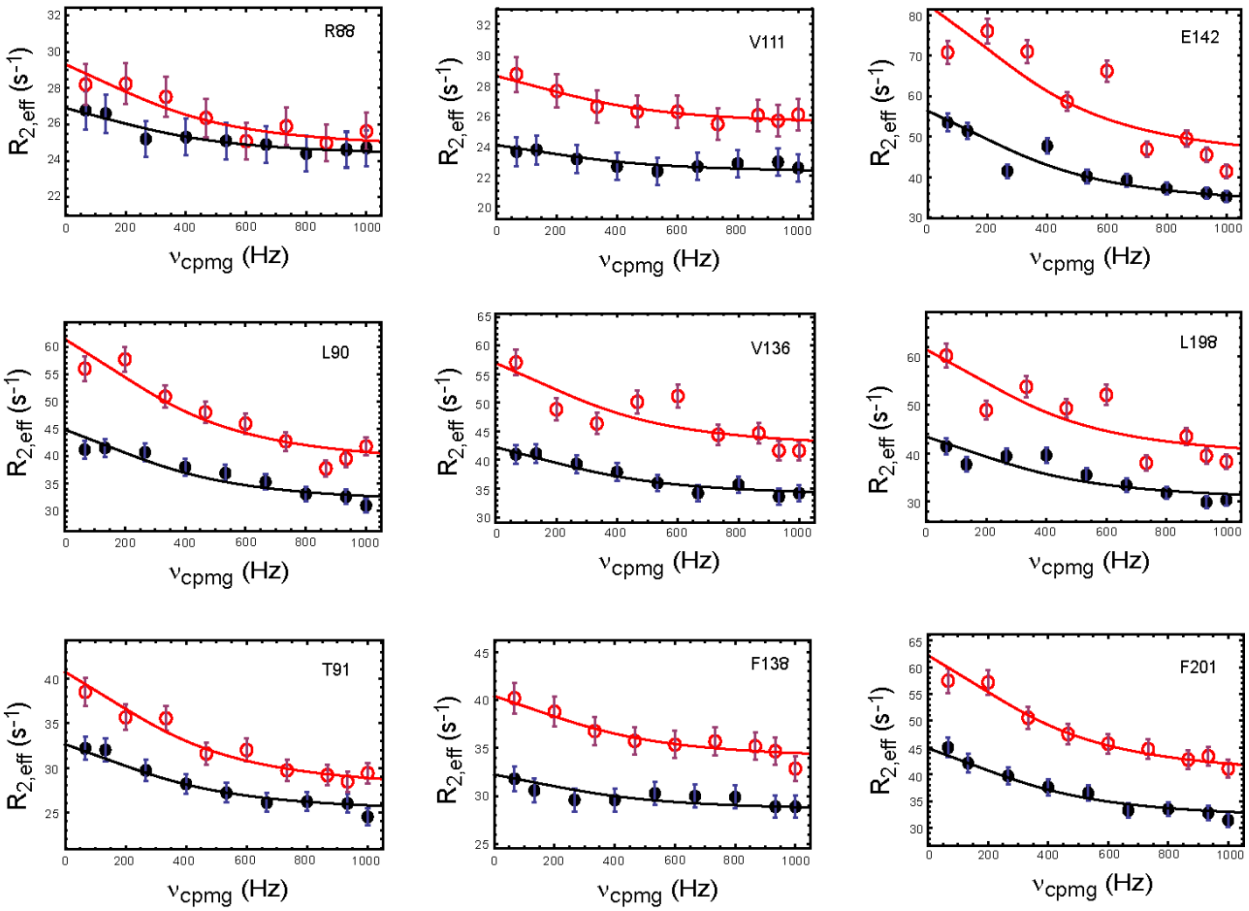

Figure S7B. NMR ^{15}N CPMG-RD data of the residues excluded from quantitative analysis (group B). Data at both field strengths were globally fit (solid lines) using the Carver-Richards equation with pre-defined k_{ex} (2459 s^{-1}) and p_{minor} (8%) values.

Supporting Figure 8

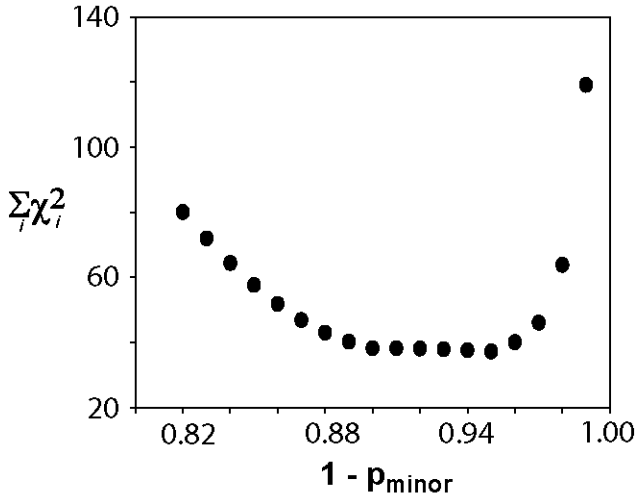

Figure S8. The χ^2 surface along a minor-species population (p_{minor}). The $\Sigma\chi^2$ corresponds to the sum of all χ^2 values of all residues in group A.

Supporting Figure 9

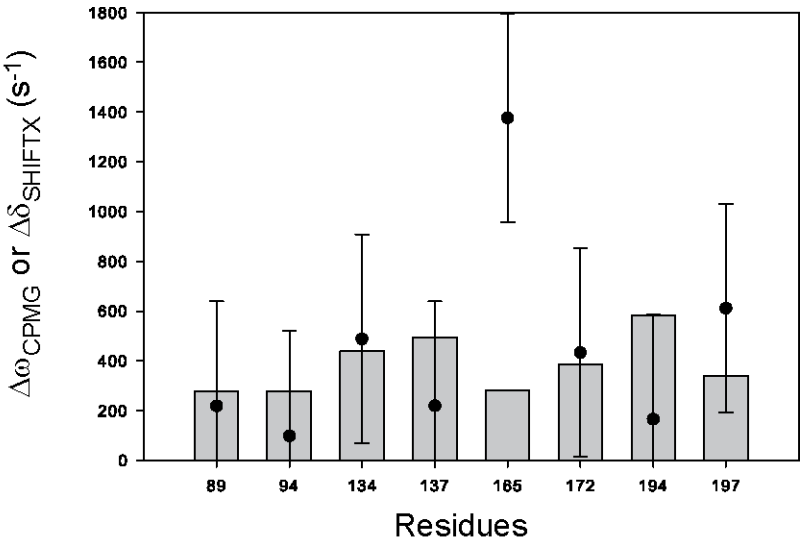

Figure S9. Comparison of $\Delta\omega_{CPMG}$ (bars) of the group-A residues with $\Delta\delta$ (closed circles) computed using SHIFTX2. The error bars correspond to RMS error of SHIFTX2-derived ^{15}N chemical shifts (1.1 ppm or 426 s^{-1} at 14.1 T). Although there exists a reasonable agreement between $\Delta\omega_{CPMG}$ and $\Delta\delta_{SHIFTX}$, relatively large RMSE of SHIFTX2-computed ^{15}N chemical shift and a small number of residues included in this comparison prevented a quantitative structural characterization of the minor species.

Supporting Figure 10

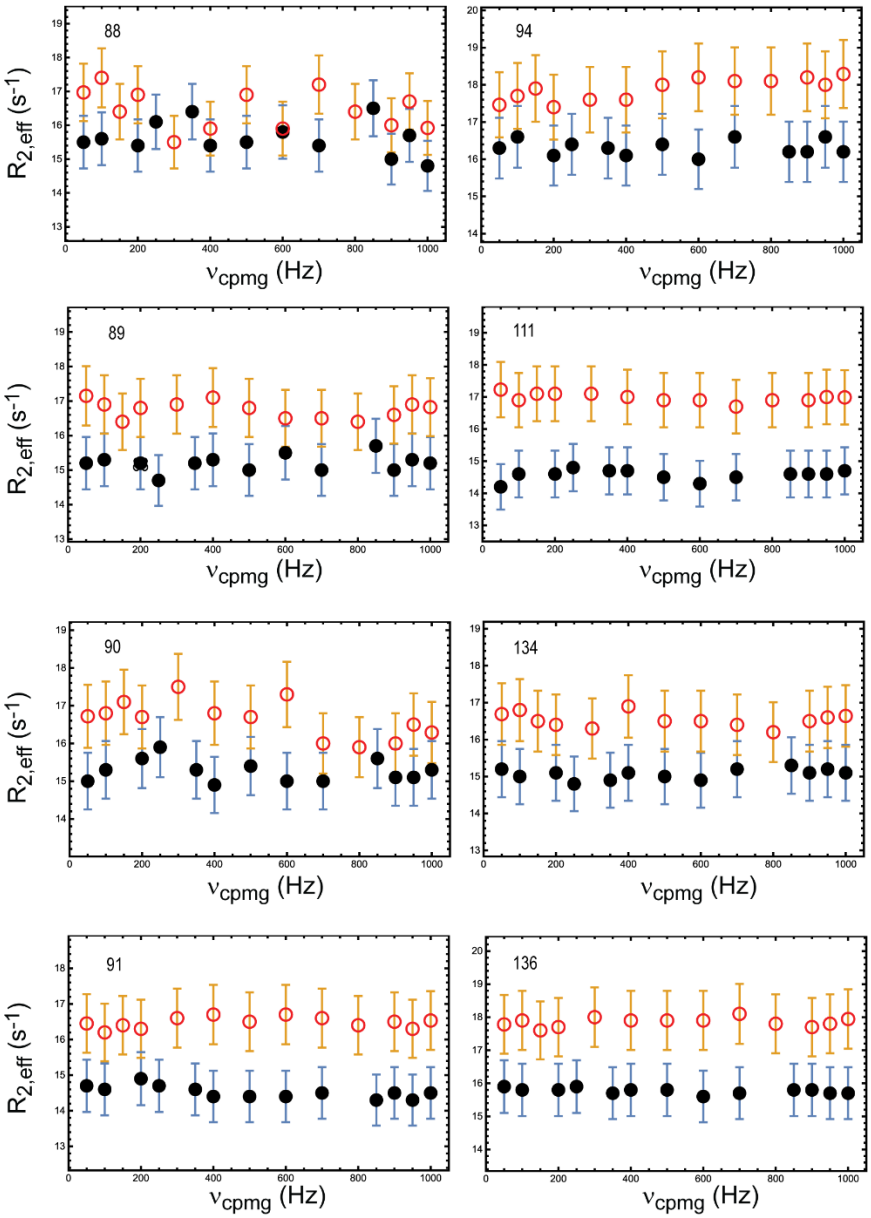

Supporting Figure 10 (continued)

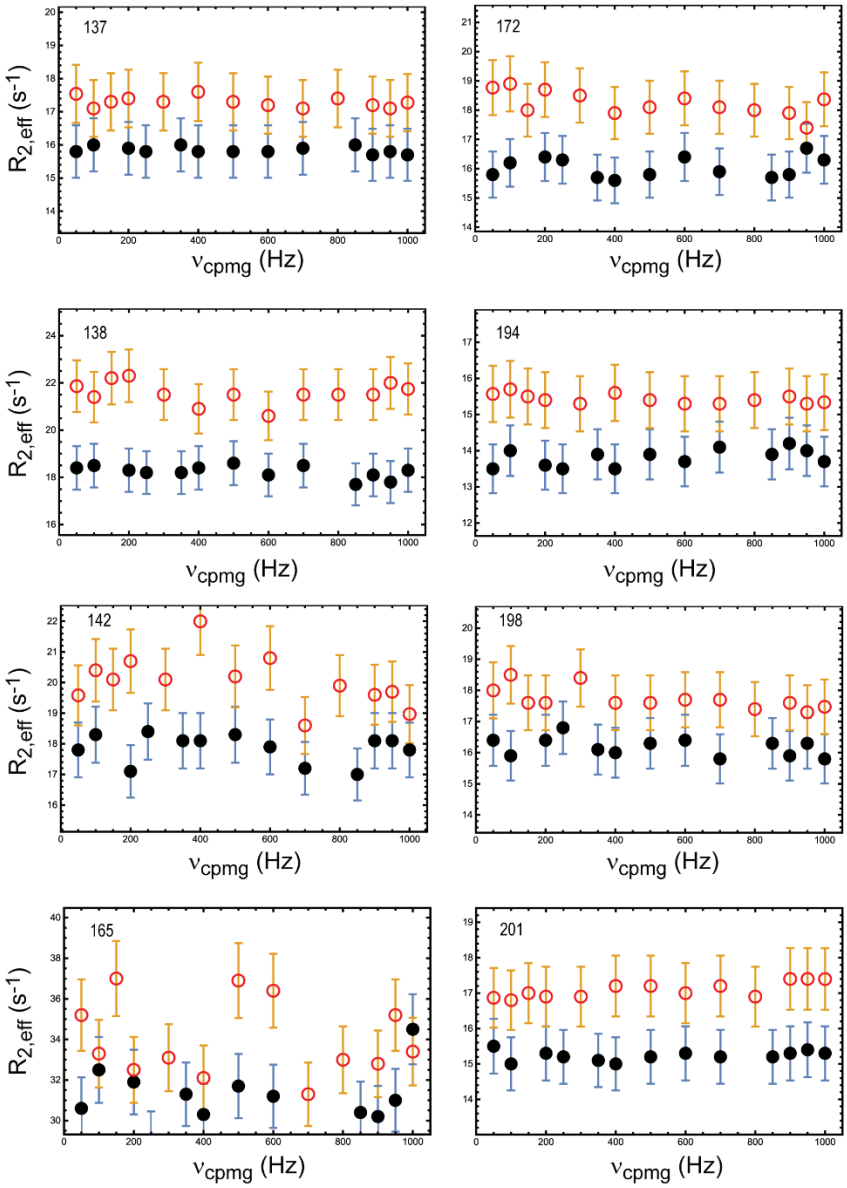

Figure S10. NMR ^{15}N CPMG-RD data of the residues in free Ud NS1^{ED}. These residues showed measurable R_{ex} in free 1918 NS1^{ED} (see Figure S7 for comparison).

.

Supporting Figure 11

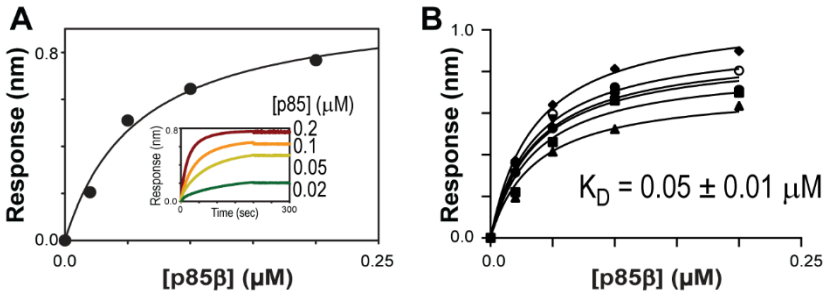

Figure S11. (**A**) A representative BLI-derived binding isotherm between surface-immobilized Ud NS1^{ED} W187A and free p85β^{iSH2} in wells. (**B**) Six replicated binding isotherms between surface-immobilized Ud NS1^{ED} W187A and free p85β^{iSH2} in wells. The binding isotherms were globally fit to obtain binding affinities (K_D).

Supporting Figure 12

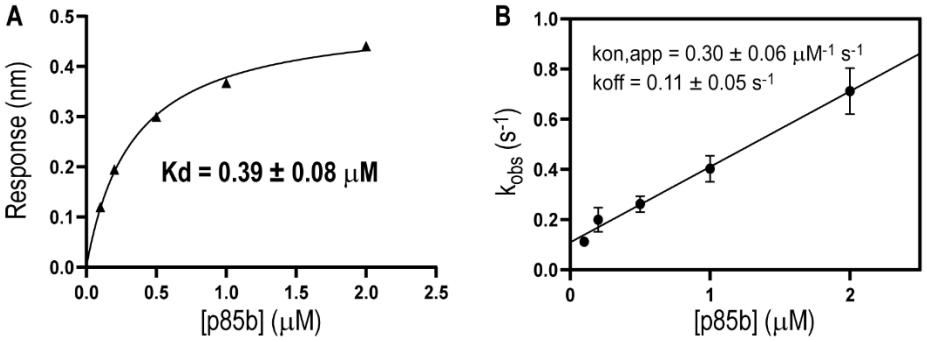

Figure S12. BLI-derived binding affinity (**A**) and kinetics (**B**) between 1918 $NS1^{ED}$-L95I/M98L and $p85\beta^{iSH2}$. The results shown in the figures are average and standard deviation of three repeated measurements.

Supporting Figure 13

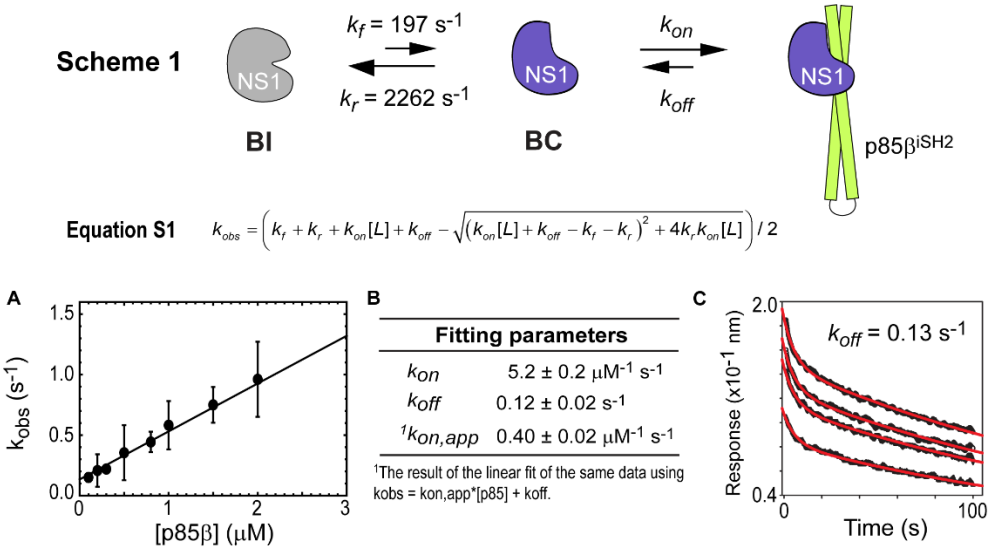

Figure S13. A schematic diagram showing the proposed two-step binding mechanism of 1918 NS1^{ED} and p85β. An analytical equation for the corresponding observed binding rate constant (k_{obs}) is shown below. (**A**) The observed rate constant k_{obs} plotted as a function of concentration of p85β^{iSH2}; this is the same data as **Figure 7A**. The solid line corresponds to the non-linear fit using equation S1 (1, 2) with k_f and k_r measured by NMR CPMG-RD. (**B**) The result of the non-linear fit. (**C**) Direct measurement of the dissociation rate constant k_{off} between 1918 NS1^{ED} and p85β^{iSH2} by BLI. Surface-immobilized NS1^{ED} was incubated with four different concentrations (2 μM, 1μM, 0.5 μM, and 0.2 μM) of p85β^{iSH2} before dissociation was initiated. Solid lines correspond to the global fit of all four traces. The fit yielded k_{off} = 0.13 ± 0.03 s^{-1}.

Supporting Figure 14

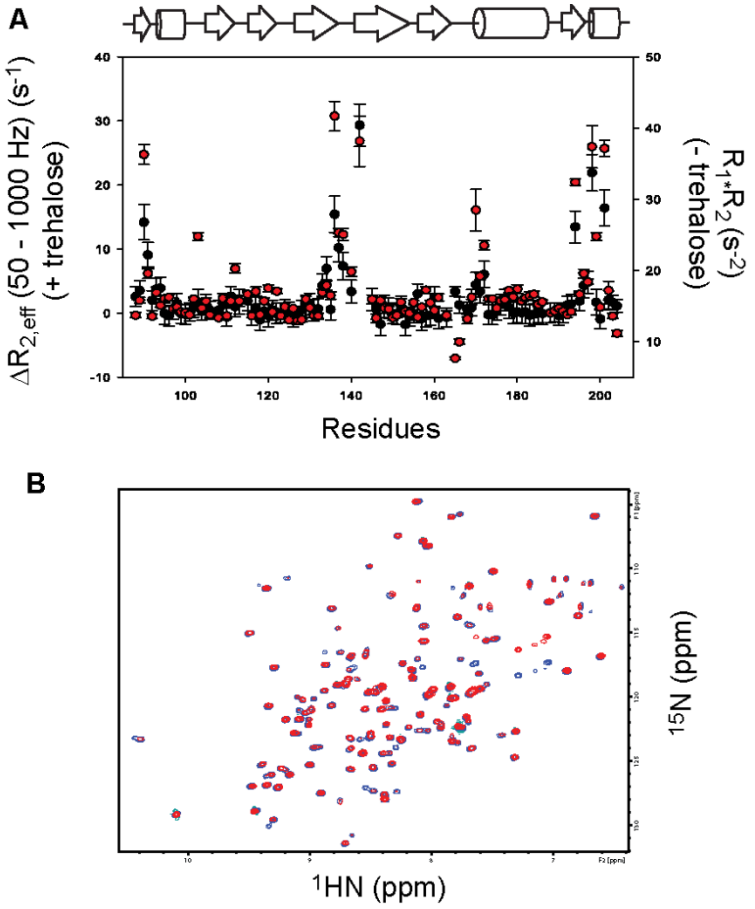

Figure S14. Trehalose does not affect the observed conformational dynamics of 1918 NS1^{ED}. (**A**) NMR ^{15}N $\Delta R_{2,eff}$ ($R_{2,eff,vcpmg = 0\ Hz} - R_{2,eff,\ vcpmg=1000\ Hz}$) values of free 1918 NS1^{ED} in the presence of 0.4 M trehalose (black circles). NMR R_1*R_2 values of free 1918 NS1^{ED} in the absence of trehalose (red circles). (**B**) Overlay of ^{1}H-^{15}N HSQC spectra of 1918 NS1^{ED} in the absence (blue peaks) and presence of trehalose (red peaks).

Supporting Figure 15

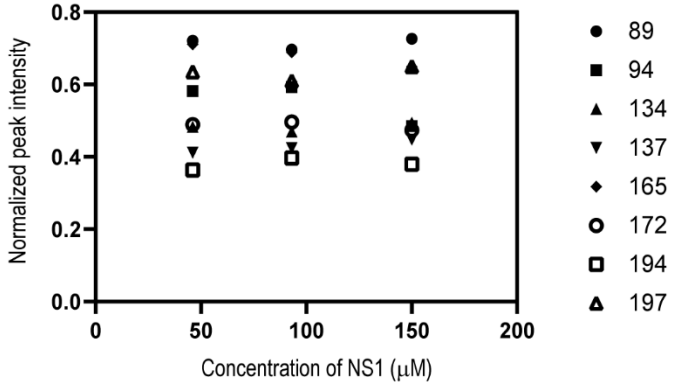

Figure S15. Concentration dependent NMR peak intensities of dynamic residues in 1918 $NS1^{ED}$. Peak intensities were normalized relative to that of non-dynamic residue (residue 99).

Supplementary Discussion

Based on our results, the simplest binding mechanism between $NS1^{ED}$ and $p85\beta^{iSH2}$ is a two-step binding through conformational selection (**Scheme 1 in Fig. S13**) (1-3), in which the binding competent (**BC**) state is responsible for the productive binding. Following the model, the reported k_{on} value is apparent k_{on} ($k_{on,app}$), which is in fact a combination of the microscopic rate constants, including k_f, k_r, and k_{on}. Direct association and dissociation rate constants, k_{on} and k_{off} (**Scheme 1 in Fig. S13**), can be estimated by nonlinear fitting of the k_{obs} vs. [p85] data using equation S1 (1) and NMR-defined k_f and k_r values. Fitting the kinetic data for 1918 NS1 yielded k_{on} and k_{off} values of 5.2 ± 0.2 $\mu M^{-1}s^{-1}$ and 0.12 ± 0.02 s^{-1}, respectively (**Fig. S13A and S13B**). Moreover, the fit k_{off} value was close to the directly measured value using BLI (**Fig. S13C**), which is a characteristic signature of a conformational selection mechanism (1). This integrated analysis of BLI-derived kinetics and NMR-derived dynamics provided a rigorous test of the binding model and supported our hypothesis in which the minor state has a conformation competent for binding. Moreover, the result demonstrated that the conformational dynamics step significantly modulated the observed binding rate constant.

Assuming that Ud $NS1^{ED}$ undergoes a subtle, but necessary, conformational exchange to bind p85β and that the NMR-detected dynamics of the two residues (H169 and T170) correspond to the motion, fitting the kinetic data of Ud NS1 using eq. S1 and NMR-determined k_f and k_r yielded k_{on} = 14.5 $\mu M^{-1}s^{-1}$ and k_{off} = 0.004 s^{-1}. However, it should be noted that the presence and role of the conformational change in Ud NS1 upon binding to $p85^{\beta iSH2}$ are uncertain due to the lack of a complex structure. Therefore, the result of the analysis remains to be validated in a future study.

References for supporting information

1. Vogt AD & Di Cera E (2012) Conformational selection or induced fit? A critical appraisal of the kinetic mechanism. *Biochemistry* 51:5894-5902.
2. Vogt AD & Di Cera E (2013) Conformational selection is a dominant mechanism of ligand binding. *Biochemistry* 52:5723-5729.
3. Hammes GG, Chang YC, & Oas TG (2009) Conformational selection or induced fit: a flux description of reaction mechanism. *Proc Natl Acad Sci USA* 106:13737-13741.